ACS APPLIED MATERIALS & INTERFACES

Research Article

www.acsami.org

Designing Self-Healing Superhydrophobic Surfaces with Exceptional Mechanical Durability

Kevin Golovin,[†,⊥,#] Mathew Boban,[‡,⊥,#] Joseph M. Mabry,[¶] and Anish Tuteja*[,†,‡,§,⊥]

[†]Department of Materials Science and Engineering, [‡]Department of Macromolecular Science and Engineering, [§]Department of Chemical Engineering, and [⊥]Biointerfaces Institute, University of Michigan, Ann Arbor, Michigan 48109, United States

[¶]Rocket Propulsion Division, Air Force Research Laboratory, Edwards Air Force Base, Edwards, California 93524, United States

Supporting Information

ABSTRACT: The past decade saw a drastic increase in the understanding and applications of superhydrophobic surfaces (SHSs). Water beads up and effortlessly rolls off a SHS due to its combination of low surface energy and texture. Whether being used for drag reduction, stain repellency, self-cleaning, fog harvesting, or heat transfer applications (to name a few), the durability of a SHS is critically important. Although a handful of purportedly durable SHSs have been reported, there are still no criteria available for systematically designing a durable SHS. In the first part of this work, we discuss two new design parameters that can be used to develop mechanically durable SHSs via the spray coating of different binders and fillers. These parameters aid in the rational selection of material components and allow one to predict the capillary resistance to wetting of any SHS from a simple topographical analysis. We show that not all combinations of sprayable components generate SHSs, and mechanically durable components do not necessarily generate mechanically durable SHSs. Moreover, even the most durable SHSs can eventually become damaged. In the second part, utilizing our new parameters, we design and fabricate physically and chemically self-healing SHSs. The most promising surface is fabricated from a fluorinated polyurethane elastomer (FPU) and the extremely hydrophobic small molecule 1H,1H,2H,2H-heptadecafluorodecyl polyhedral oligomeric silsesquioxane (F-POSS). A sprayed FPU/F-POSS surface can recover its superhydrophobicity even after being abraded, scratched, burned, plasma-cleaned, flattened, sonicated, and chemically attacked.

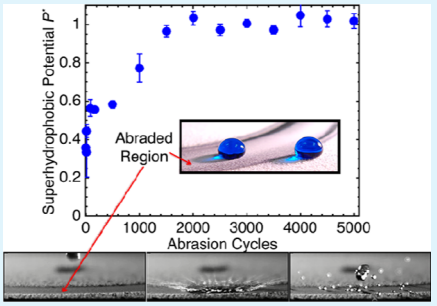

KEYWORDS: *superhydrophobic, wettability, durability, self-healing, coatings*

INTRODUCTION

Superhydrophobic surfaces (SHSs) have garnered much attention over the last few decades for their ability to be self-cleaning,[1] drag-reducing,[2] stain-resisting,[3] and antifouling.[4] By trapping pockets of air in their porous texture, SHSs display water contact angles >150° and low roll-off angles.[5] The design and optimization of such surfaces have been well studied.[1−17] However, most natural and artificial SHSs suffer from poor mechanical durability, as their fragile and porous surface texture can be easily removed even by the swipe of a finger.[12] Only a few SHSs have been reported to exhibit mechanical durability, as characterized by sand impact,[18−22] rubbing with a soft cloth,[3,23−25] tape peel tests,[7,19,26−28] or sandpaper abrasion.[9,12,14−16,19,24,29−40] However, all such reports present single material systems. The development of design criteria to aid in the systematic fabrication of durable SHSs, generalizable to multiple chemistries or fillers, is expected to be extremely useful to the field. In the first part of this work, we aim to develop such criteria.

Even the most durable SHSs will eventually become damaged by extreme or repeated mechanical abrasion, which damages their low surface energy or texture. SHSs that can regenerate their surface texture and chemistry,[41−43] akin to the lotus leaf's ability to regenerate its nanostructured wax,[1] would be highly desirable. Herein, we also report mechanically durable SHSs that exhibit physical and chemical self-healing. The developed surfaces can fully recover their water-repellency even after being abraded, scratched, burned, plasma cleaned, flattened, sonicated, and chemically attacked. These surfaces, and the design parameters used to develop them, may find immediate usage in a wide range of academic and industrial sectors across the globe.

DESIGNING A DURABLE SHS: CHEMISTRY AND MISCIBILITY

The lowest possible surface energy, γ_{SV}, is achieved with a monolayer of $-CF_3$ groups ($\gamma_{SV} \approx 6$ mN/m).[44] Chemically grafting such monolayers requires specific substrate chemistry. Moreover, the thin monolayer only renders the uppermost surface hydrophobic, and any surface degradation will expose the higher surface energy material underneath. In contrast, the incorporation of highly perfluorinated compounds within a coating allows one to achieve equally low surface energies

Received: December 5, 2016
Accepted: March 7, 2017
Published: March 7, 2017

DOI: 10.1021/acsami.6b15491
ACS Appl. Mater. Interfaces 2017, 9, 11212−11223

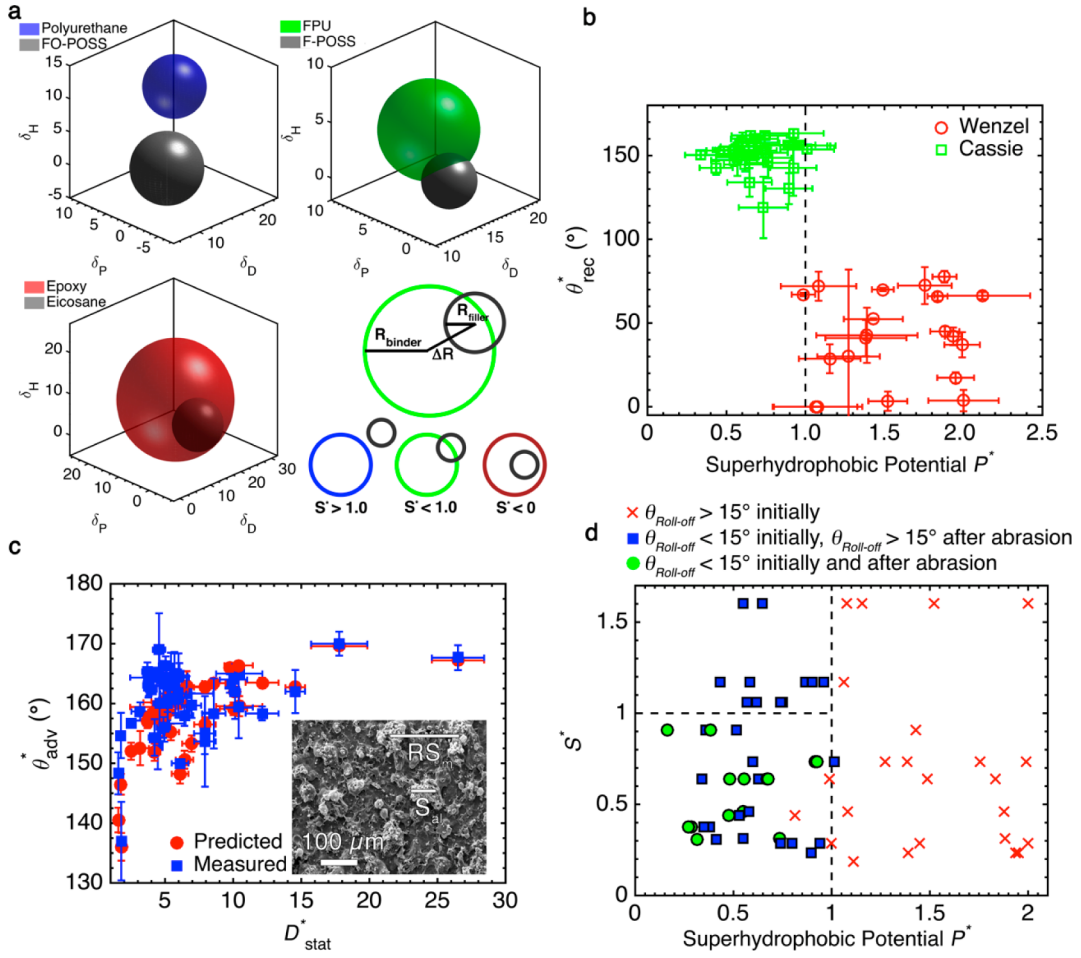

Figure 1. Designing SHSs. (a) Visualization of the S^* parameter for three binders in 3D Hansen space. FO-POSS: fluorooctyl polyhedral oligomeric silsesquioxane. FPU: fluorinated polyurethane. F-POSS: fluorodecyl polyhedral oligomeric silsesquioxane. (b) Apparent receding contact angle versus the P^* parameter. The sharp transition at $P^* = 1.0$ denoted a Young's contact angle of 120°. (c) Measured and predicted apparent advancing contact angles versus the developed statistical porosity parameter. This plot includes all the different systems from Table 1. The inset shows a SEM micrograph of the FPU/F-POSS sprayed surface, with representative RS_m and S_{al} values indicated. (d) Phase diagram for all the surfaces developed in this work (see Table 1). Only surfaces with $P^* < 1.0$ can be superhydrophobic ($\theta_{roll\text{-}off} < 15°$, 25 μL), and additionally only surfaces with $0 < S^* < 1.0$ can be mechanically durable ($\theta_{roll\text{-}off} < 15°$ after 100 abrasion cycles). The non-SHS that exhibited $P^* < 1.0$ was a blend of FPU/FO-POSS. For this blend, $\theta = 91°$, although the sprayed texture required $\theta_c = 114°$. This is an example where the texture is sufficient to produce a SHS, but the chemistry does not exhibit low enough surface energy.

without the need for chemical grafting.[45,46] Moreover, these unbound species can diffuse to the surface, restore the low surface energy after mechanical or chemical attack (discussed later), and reduce the formation of hydrophilic defects upon damage.[12] Such coatings can be universally applied to any substrate and impart low surface energy throughout the entire thickness of the coating. In this work, we fabricated a library of SHSs using sprayed blends of polymeric binders and hydrophobic fillers. Because of its low surface energy ($\gamma_{SV} \approx 10$ mN/m), we primarily focus on systems incorporating 1H,1H,2H,2H-heptadecafluorodecyl polyhedral oligomeric silsesquioxane (F-POSS),[45] although the developed design parameters are generalizable to other material systems, as shown here. Spray coating was chosen as the primary methodology for the application of the superhydrophobic coatings. Spray coating is inexpensive, scalable, and allows control over the surface energy and texture of our coatings via simple changes in experimental parameters.

As the fillers used in this work are soluble small molecules rather than nondeformable particles, they cannot induce texture directly. We observed the microscale texture formation during spray coating to be strongly dependent on the miscibility between the binder and filler components. Chemically similar blends yielded smooth, nonsuperhydrophobic coatings, but very chemically dissimilar blends yielded highly superhydrophobic, but mechanically fragile coatings (discussed later). This motivated the quantitative study of the miscibility and its relation to durable superhydrophobicity.

The cohesive energy of any material species can be broken into its dispersive, polar, and hydrogen bonding Hansen solubility parameters, (δ_D, δ_P, δ_H).[47] A miscibility sphere can be experimentally constructed for any compound, with its center at some point in a 3D space defined by these three solubility parameters, and its volume encompassing all good solvents and excluding all nonsolvents. We determined the miscibility spheres for several hydrophobic fillers and a wide variety of binders (Figure 1a) by screening their solubility in a large number of solvents (Supporting Information, Tables S1−S3). The overlap between the Hansen spheres of the binder and filler is indicative of their chemical similarity and the extent to

DOI: 10.1021/acsami.6b15491
ACS Appl. Mater. Interfaces 2017, 9, 11212−11223

Table 1. Surface Properties of Coatings in This Work before and after 100 Rotary Taber Abrasion Cycles

base	% F-POSS	P^*	D^*_{stat}	initial θ^*_{adv} [°]	initial θ^*_{rec} [°]	initial $\theta_{roll\text{-}off}$ [°]	100 cycle θ^*_{adv} [°]	100 cycle θ^*_{rec} [°]	100 cycle $\theta_{roll\text{-}off}$ [°]	100 cycle mass loss [%]
Neverwet		1.79	7.4	165	162	1	132	37	54	17
Ultra Ever Dry		1.36	4.0	161	152	1	155	0	90	14
Cytonix WX 2100		1.04	1.4	164	156	18	122	77	90	6
FPU (S^* = 0.64)	0	1.84	7.2	115	66	55				
FPU	1	0.99	14.3	106	67	90	106	63	90	1
FPU	3	1.49	25.5	121	66	90	122	78	76	3
FPU	5	0.31	1.5	148	112	62	151	102	75	8
FPU	10	0.34	2.5	162	150	10	159	124	22	20
FPU	15	0.48	3.9	165	159	2	161	154	2	32
FPU	20	0.56	3.5	163	153	5	161	144	10	40
FPU	25	0.67	6.4	166	153	2	164	152	2	86
FPU	30	0.68	4.8	165	160	2	163	144	3	81
FPU	35	0.63	4.4	160	151	1	146	113	24	56
FPU-PG (S^* = 1.06)	5	0.62	5.3	163	145	8	153	98	81	44
FPU-PG	10	0.57	8.2	161	152	7	158	116	57	40
FPU-PG	15	0.75	4.7	162	148	7	161	113	90	27
FPU-PG	20	0.74	5.6	164	151	3	159	123	40	26
PMMA (S^* = 1.17)	0	1.06	5.1	155	0	90				
PMMA	2	0.76	5.5	160	83	14	135	0	90	109
PMMA	5	0.43	4	160	143	11	159	123	35	99
PMMA	10	0.58	3.4	163	153	7	159	128	24	104
PMMA	35	0.90	5.9	166	156	2	162	127	26	129
PMMA	50	0.86	4.2	164	156	0	127	84	63	100
SF-100 (S^* = 0.74)	0	1.99	2.9	93	37	64				
SF-100	5	1.38	3	129	41	90				
SF-100	10	1.75	2.9	140	72	83				
SF-100	15	1.27	4.5	158	123	13	167	113	37	22
SF-100	20	1.01	3.8	163	157	1	165	133	21	30
SF-100	25	0.92	3.5	169	163	0	166	164	1	55
SF-100	35	0.60	7	167	159	2	145	107	34	38
PDMS (S^* = 0.32)	0	1,88	3.8	123	45	90				
PDMS	15	0.73	5.4	154	119	47	158	137	10	20
PDMS	30	0.55	5.4	160	153	4	157	0	66	46
PFPE (S^* = 0.46)	0	1.88	18.6	113	78	53				
PFPE	5	2.12	0.5	127	66	66				
PFPE	15	1.08	7	155	72	47	163	20	90	45
PFPE	25	0.55	3.7	156	147	7	163	142	8	33
PFPE	35	0.58	4.1	165	153	2	164	0	90	100
Vytaflex (S^* = 1.60)	0	2.00	1	73	4	90				
Vytaflex	1	1.52	9.6	149	0	90				
Vytaflex	5	1.08	4.5	150	0	90				
Vytaflex	10	1.15	3.1	135	29	90				
Vytaflex	15	0.65	4.5	158	134	11	159	55	39	28
Vytaflex	35	0.55	5.2	160	150	2	161	130	17	
PS 45 (S^* = 0.48)	0	1.15	26.6	157	123	14				
PS 45	15	0.60	1.9	157	131	14	156	114	37	26
PS 45	25	0.58	1.4	155	142	15	152	111	38	14
PS 1.2 (S^* = 0.48)	15	0.94	8.5	159	153	0				100
PIB (S^* = 0.19)	0	1.27	19.3	118	61	90				
PIB	15	1.18	10.4	164	143	14	161	118	90	48
Araldite (S^* = 0.23)	0	1.95	2.9	101	17	90				
Araldite	5	1.94	12.5	128	43	90	127	62	87	
Araldite	15	1.39	1	137	43	90	132	69	90	3
Araldite	25	0.89	9	158	130	14	158	16	90	25
Desmophen 670BA (S^* = 0.91)	0	1.43	41.9	85	49	90				0
Desmophen 670BA	2.5	0.52	8.9	161	141	8	148	94	74	17
Desmophen 670BA	5	0.36	7.8	166	157	5	159	125	23	20
Desmophen 670BA	10	0.38	8.4	166	160	4	162	129	16	24
Desmophen 670BA	15	0.17	2.3	165	156	9	164	162	2	27

DOI: 10.1021/acsami.6b15491
ACS Appl. Mater. Interfaces 2017, 9, 11212−11223

Table 1. continued

base	% FO-POSS	P^*	D^*_{stat}	initial θ^*_{adv} [°]	initial θ^*_{rec} [°]	initial $\theta_{roll\text{-}off}$ [°]	100 cycle θ^*_{adv} [°]	100 cycle θ^*_{rec} [°]	100 cycle $\theta_{roll\text{-}off}$ [°]	100 cycle mass loss [%]
FPU (S^* = 0.44)	15	0.81	8.9	141	66	90	137	68	90	4
FPU	25	0.53	7.2	163	149	9	161	124	30	12
FPU	35	0.48	7.0	162	153	4	162	146	14	15

base	% IB-POSS	P^*	D^*_{stat}	initial θ^*_{adv} [°]	initial θ^*_{rec} [°]	initial $\theta_{roll\text{-}off}$ [°]	100 cycle θ^*_{adv} [°]	100 cycle θ^*_{rec} [°]	100 cycle $\theta_{roll\text{-}off}$ [°]	100 cycle mass loss [%]
FPU (S^* = 0.31)	25	0.41	5.1	165	130	15	140	75	90	9
FPU	30	0.31	4.9	164	144	5	165	132	15	17
Desmophen 670BA (S^* = 0.37)	2.5	0.52	5.7	139	57	90	129	46	90	5
Desmophen 670BA	5	0.36	8.6	158	96	81	137	46	90	8
Desmophen 670BA	10	0.35	6.6	164	142	13	160	66	90	20
Desmophen 670BA	15	0.38	7.8	163	139	14	150	91	61	16
Desmophen 670BA	25	0.28	5.8	165	148	8	165	136	15	21
Desmophen 670BA	30	0.27	5.8	166	151	10	165	155	6	24

base	% eico-sane	P^*	D^*_{stat}	initial θ^*_{adv} [°]	initial θ^*_{rec} [°]	initial $\theta_{roll\text{-}off}$ [°]	100 cycle θ^*_{adv} [°]	100 cycle θ^*_{rec} [°]	100 cycle $\theta_{roll\text{-}off}$ [°]	100 cycle mass loss [%]
CNR (S^* = 0.29)	0	2.00	18.3	93	78	90				
CNR	25	1.45	11.3	157	82	84				
CNR	30	1.00	3.5	162	87	71				
CNR	35	0.74	4.3	153	141	14	162	92	33	2
CNR	40	0.80	3.4	148	137	15	163	113	38	3
CNR	50	0.94	6.5	160	146	11	164	77	90	11

which they phase separate and form texture during the spray-coating process. To quantify a polymer's miscibility with the filler, we developed the miscibility parameter S^*, which is given as

$$S^* = \frac{\Delta R - R_{binder} + R_{filler}}{2R_{filler}} \quad (1)$$

Here, ΔR is the distance in 3D solubility space between the centers of the filler's sphere and the binder's sphere, with their radii denoted by R_{filler} and R_{binder}, respectively.

Similar to Hansen's relative energy difference[47] value, S^* is defined such that the filler is completely immiscible with a binder when the two spheres do not overlap ($S^* > 1.0$, also see schematic in Figure 1a). Alternately, binders with $S^* < 0$ have solubility spheres that completely encompass the filler's sphere and are hence fully miscible (at a given concentration, see Figure S5). In between these two extremes is the regime of partial miscibility, which turns out to have far-reaching consequences for the sprayed superhydrophobic surface's durability.

The S^* parameter allows one to predict if the filler will phase separate from the binder during spray coating. This phase separation manifests in the sprayed surface's root−mean−squared roughness, S_q. For example, we determined the solubility spheres for a polyurethane and an epoxy, which are both commonly used hydrophilic adhesives (Tables S2 and S3). For the epoxy, $S^* \approx 0.2$ with F-POSS, and an epoxy+5 wt % F-POSS blend, when sprayed, resulted in a smooth surface with S_q = 0.8 μm. Conversely, for the polyurethane, $S^* \approx 1.6$, and a polyurethane+5 wt % F-POSS blend, when sprayed in the exact same manner (methods), resulted in a very rough surface (S_q = 41 μm). Thus, immiscibility alone can induce roughness during the spray coating process. However, a large S_q does not guarantee superhydrophobicity.[48]

DESIGNING A SHS: SURFACE TEXTURE

Water on SHSs can exist in the Cassie−Baxter state, in which air pockets are trapped in the surface's porous texture.[49] However, water can displace these air pockets, which leaves the surface in a wetted, Wenzel state.[50] SHSs should ideally be designed such that the Cassie−Baxter state is energetically preferred.[1] We developed a method to predict when the Cassie−Baxter state would be energetically favorable over the Wenzel state using only the topographical statistics of a given surface. Because each binder/filler combination exhibited a distinct, characteristic surface morphology, we wished to develop universal metrics that characterize surfaces with widely varying topographies. To do so, we measured three statistical surface properties (methods): peak periodicity, RS_m, autocorrelation length, S_{al}, and Wenzel roughness, r (the ratio of the actual surface area to its projected area).[50] RS_m represents the length along the surface between large surface features and can be thought of as the center-to-center distance between texture elements.[51] S_{al} denotes the length at which a surface no longer exhibits self-similarity and can be thought of as the average size of the largest texture features. We, therefore, can define the statistical porosity D^*_{stat} of the surface as (inset, Figure 1c)

$$D^*_{stat} = (RS_m/S_{al})^2 \quad (2)$$

where the second power is added to convert from properties measured along one-dimensional height profiles to the porosity of a two-dimensional surface.[11] Larger values of D^*_{stat} indicate surfaces with higher porosity.

For the Cassie−Baxter state to be favored over the wetted Wenzel state, it must be the global energy minimum.[52] For a given surface topography, the free energies of the two states can be balanced. The nonwetted state is energetically preferred only if the Young's contact angle of the material, θ, exceeds a critical value, θ_c. This critical Young's contact angle is given by $\cos\theta_c = (\phi_s - 1)/(r - \phi_s)$,[52] where ϕ_s is the fraction of solid in contact

DOI: 10.1021/acsami.6b15491
ACS Appl. Mater. Interfaces 2017, 9, 11212−11223

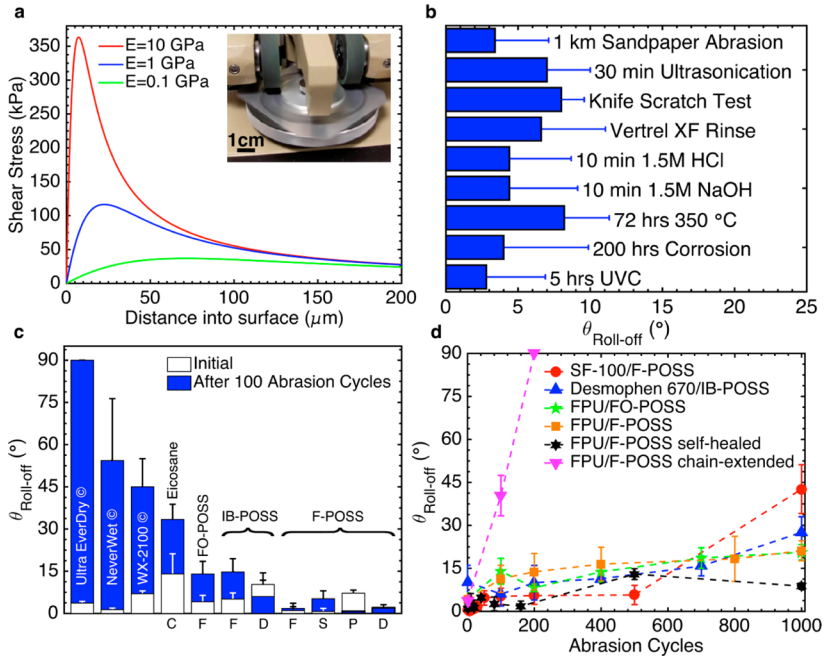

Figure 2. Mechanical durability. (a) Shear stress experienced during Taber abrasion as a function of depth into the coating. The values are found using Hertzian contact mechanics (see Supporting Information). The inset shows the Taber abrasion machine. (b) Additional durability characterizations that the FPU/F-POSS coating could withstand without self-healing. (c) Roll-off angles for three commercially available SHSs and eight of the SHSs fabricated in this work (with $S^* < 1.0$), initially and after 100 abrasion cycles. C, chlorinated rubber; F, FPU; D, Desmophen 670BA; S, SF-100; P, PFPE. (d) Droplet roll-off angles for four representative, durable SHSs fabricated in this work. The data for the propylene glycol chain extended FPU/F-POSS and the self-healed FPU/F-POSS are also shown. All roll-off experiments used 25 μL droplets.

with water (note $D^*_{stat} \approx \phi_s^{-1}$). Stated differently, by recalling that Young's water contact angles cannot exceed 120° even on a fully perfluorinated monolayer,[10] there exists some minimal texture that any surface, regardless of surface chemistry, must exhibit to achieve an energetically favorable Cassie–Baxter state. Substituting this maximum contact angle as θ_c yields

$$\cos\theta_c = \cos 120^\circ = (1/D^*_{stat} - 1)/(r - 1/D^*_{stat})$$

or

$$-0.5 = (1 - D^*_{stat})/(rD^*_{stat} - 1)$$

We can then define a surface's superhydrophobic potential, P^*, such that only for values of $P^* < 1.0$ is the Cassie–Baxter state the global energy minimum. Doing so yields

$$P^* = 2(D^*_{stat} - 1)/(rD^*_{stat} - 1) \quad (3)$$

For any surface that exhibits $P^* > 1.0$, the wetted state is energetically preferred, regardless of surface chemistry. Note that water can exist in a metastable Cassie–Baxter state through the addition of re-entrant texture,[10] and hence, a value of $P^* > 1.0$ does not necessarily indicate wetting. P^* is useful because surfaces are often created with a given topography and then subsequently rendered superhydrophobic by application of a low surface energy layer on top.[1] As such, measuring P^* allows one to determine a priori if such a surface will become superhydrophobic before such a (often expensive) low surface energy monolayer is applied. Moreover, if a surface is superhydrophobic in spite of a $P^* > 1.0$ value, one can say with certainty that water will exist in a metastable state, and such a surface should be used with caution. By measuring the dynamic contact angles on many surfaces, both wetted and nonwetted, we probed the effectiveness of P^*.

When water initially advances on a SHS, it displays a maximum apparent contact angle, θ^*_{adv}.[53] If any texture elements become wetted, the apparent angle at which water recedes, θ^*_{rec}, will decrease. Thus, θ^*_{adv} is a measure of the SHS's inherent porosity (i.e., fraction of air pockets), ignoring how stable the air pockets may be, and θ^*_{rec} gives an indication of their stability.[54] We measured θ^*_{rec} for more than 50 combinations of F-POSS and various polymeric binders, as a function of P^* (Figure 1b). These binders included both cross-linked networks, such as different urethanes, acrylates, epoxies, and cyanoacrylates, as well as linear polymers such as polystyrene, poly(methyl methacrylate) and polyisobutylene (Methods, Table 1). We observed a high θ^*_{rec} only for systems with a stable Cassie–Baxter state, that is, $P^* < 1.0$. This was confirmed by the sharp jump in θ^*_{rec} at a value of $P^* = 1.0$. The specific value of $P^* = 1.0$, corresponding to a Young's contact angle $\theta \approx 120°$, indicated that all the surfaces had a high percentage of F-POSS at the solid–liquid interface, although there were vast differences in topography. Thus, we were able to predict if an F-POSS-containing surface could be superhydrophobic solely by measuring P^*. Without measuring P^*, there is no easy way to determine if a randomly textured surface has the potential to become superhydrophobic, a priori. Moreover, for surfaces with $P^* < 1.0$, recasting the Cassie–Baxter relation[49] in terms of D^*_{stat} effectively predicted θ^*_{adv} (Figure 1c). We observed that the predictive power of D^*_{stat} and P^* extended to other SHSs not containing F-POSS. These SHSs included polymer blends with other hydrophobic fillers like eicosane, octa-isobutyl POSS (IB-POSS), and fluoro-octyl POSS (FO-POSS), as well as other SHSs such as three commercially available superhydrophobic formulations (Methods, Tables S1–S3), lithographically fabricated microstructures,[55] textured metals treated with self-assembled monolayers,[56,57] and binders filled with hydrophobic

DOI: 10.1021/acsami.6b15491
ACS Appl. Mater. Interfaces 2017, 9, 11212–11223

particles.[58] As such, the design parameters developed in this work are applicable to SHSs produced using a wide range of binders, fillers, and fabrication techniques.

For each binder (fixed S^*), we varied P^* by adjusting the amount of hydrophobic filler in the blend. Combining the S^* and P^* parameters allowed us to construct a phase diagram for the different possible surfaces created when spraying the binder/filler blends (Figure 1d). Here we denote surfaces with a red "×" when the water roll-off angle was $\theta_{roll\text{-}off} > 15°$ (not superhydrophobic) and surfaces that exhibited $\theta_{roll\text{-}off} < 15°$ (superhydrophobic) as blue squares. These two regions were demarcated by a line at $P^* = 1.0$, that is, we never observed a SHS for which $P^* > 1.0$.

Low surface energy species are known to preferentially migrate to the solid−air interface.[59] For binders with $S^* > 1.0$, the final surface was always very mechanically weak, with a powdery consistency, because the filler was completely immiscible with such binders. Green circles in Figure 1d denote surfaces that remained superhydrophobic after mechanical abrasion (discussed later). These mechanically durable SHSs were only observed when a binder exhibited partially miscibility with the filler ($S^* < 1.0$), that is, we never observed a durable SHS with $S^* > 1.0$. Finally, we note that increasing the amount of filler within a sprayed blend was not always efficacious. As the binder can be much more mechanically resilient than the filler molecules, any excess filler within the blend, beyond what is required to achieve superhydrophobicity ($P^* < 1.0$), can lower the overall durability. For example, a perfluorinated polyether, PFPE, with 25 wt % F-POSS remained superhydrophobic after abrasion, but PFPE with 35 wt % F-POSS did not, although the S^* and P^* values were equivalent. Overall, choosing components that satisfy $S^* < 1.0$ helps to ensure that the final surface will be durable, and choosing a sufficient filler content such that $P^* < 1.0$ assures that the surface will be highly water repellent.

DURABILITY OF SHSS: MECHANICAL ABRASION

We utilized the industry standard of rotary Taber abrasion to evaluate the mechanical durability of our sprayed binder/filler blends. The stresses generated by Taber abrasion can be found using a cylinder−cylinder Hertzian contact mechanics analysis (Figure S2).[60] Depending on the elastic modulus of the coating, the exerted shear stress ranged from tens to hundreds of kPa (Figure 2a). Considering the porosity of the surface, the texture elements experienced shear stresses on the order of a few MPa. This is similar or greater than the less systematic durability characterization techniques employed in the literature.[9,12,14−16,19,24,29−40] For example, in a recent report,[16] the authors' durable SHS was abraded with sandpaper along a total length of 800 cm, without degradation of high contact angle. We reproduced such an evaluation for our FPU/F-POSS blend, which maintained high contact angles, as well as low roll-off angles, even after 1 km (100 000 cm) of abrasion using the same sandpaper and applied load (Figure 2b, Figure S2b). Thus, we have good confidence in claiming that the surfaces created in this work can also withstand the other metrics of mechanical durability reported elsewhere.

One-hundred Taber abrasion cycles sufficiently differentiated durable and nondurable SHSs, that is, nondurable surfaces were either completely removed or water wet the remaining coating, after 100 abrasion cycles. Only surfaces that exhibited $\theta_{roll\text{-}off} < 15°$ after 100 abrasion cycles are shown as green circles in Figure 1d. All such surfaces exhibited partial miscibility with the hydrophobic fillers ($0 < S^* < 1.0$). We then continued Taber abrasion of our partially miscible blends (Table 1). We compared the durability of these systems to three commercially available, and purportedly durable, SHSs (Figure 2c). None of the commercial coatings maintained a low $\theta_{roll\text{-}off}$ after 100 abrasion cycles. We extended the abrasion testing of our binder/filler blends exhibiting $S^* < 1.0$ and found them to be quite resilient to mechanical wear (Figure 2d). Although all other evaluated SHSs became wettable within 100 abrasion cycles, the nonwetting properties of our surfaces endured significantly longer. When blended with F-POSS, coatings incorporating the PFPE, SF-100, and FPU binders remained superhydrophobic for up to about 400, 500, and 800 Taber abrasion cycles, respectively. Combinations of the polyurethane Desmophen 670BA and IB-POSS or the FPU and FO-POSS both exhibited $\theta_{roll\text{-}off} < 15°$ for ∼800 cycles. In fact, all such systems only became wettable once almost the entire coating was abraded away. For example, a 100 μm-thick FPU/F-POSS coating maintained $\theta_{roll\text{-}off} < 15°$ even when > 90 μm of its thickness was removed. Note that the coating mass loss was not linear with the number of abrasion cycles; large aggregates were removed first. Abrasion of smooth FPU/F-POSS blends and other partially miscible systems ($S^* \approx 0.4-0.9$), deposited by alternate means (Methods), confirmed that the abrasion process did not induce superhydrophobicity ($P^* \approx 1.3-1.9$) after abrasion (see Figure S3). Rather, only the SHSs fabricated from partially miscible components maintained $P^* < 1.0$ (Figure 2d, Figure S4) during abrasion, whereas fully miscible ($S^* < 0$) and fully immiscible ($S^* > 1.0$) systems did not.

As further proof that partial miscibility is required for mechanically durable SHSs, we chain extended the FPU by incorporating propylene glycol into the cross-linked network (Methods). The chain-extended FPU exhibited a three-fold increase in elastic modulus and a 12% reduction in mass loss during abrasion of the smooth binder (no F-POSS), as compared to unmodified FPU. However, the increased number of urethane linkages altered the Hansen sphere for the cross-linked network by changing the miscibility with F-POSS from $S^* \approx 0.6$ to $S^* \approx 1.1$. As such, although a sprayed blend of FPU +15 wt % F-POSS ($P^* = 0.48$) remained superhydrophobic after 800 abrasion cycles, a sprayed blend of the chain extended FPU+15 wt % F-POSS ($P^* = 0.56$) was no longer superhydrophobic after only 100 abrasion cycles (Figure 2d). This counterintuitive result emphasizes the fact that the binder with the correct miscibility ($0< S^* < 1.0$), not the most mechanically durable binder, can yield the most mechanically durable SHSs. Moreover, the blend of FPU/F-POSS also withstood a host of other potentially damaging exposures (Methods). After ultrasonication, a fluoro-solvent rinse, acid and base submersion, knife scratching (Movie 3), accelerated weathering, ultraviolet exposure, and being held at 350 °C for 3 days, the coating always maintained $\theta_{roll\text{-}off} < 10°$ (Methods, Figure 2b).

PHYSICAL AND CHEMICAL SELF-HEALING SHSS

In the remainder of this work, we focus on our most durable coating, the FPU binder blended with 15 wt % F-POSS. Because of the surface migration of F-POSS upon heating and the elastomeric ($T_g \ll$ room temperature) nature of the FPU, the fabricated coating can both chemically and physically self-heal. For example, the as-abraded coating maintained $\theta_{roll\text{-}off} < 15°$ up to about 800 abrasion cycles. Beyond this, $\theta_{roll\text{-}off}$ increased with the number of abrasion cycles. However, if the

DOI: 10.1021/acsami.6b15491
ACS Appl. Mater. Interfaces 2017, 9, 11212−11223

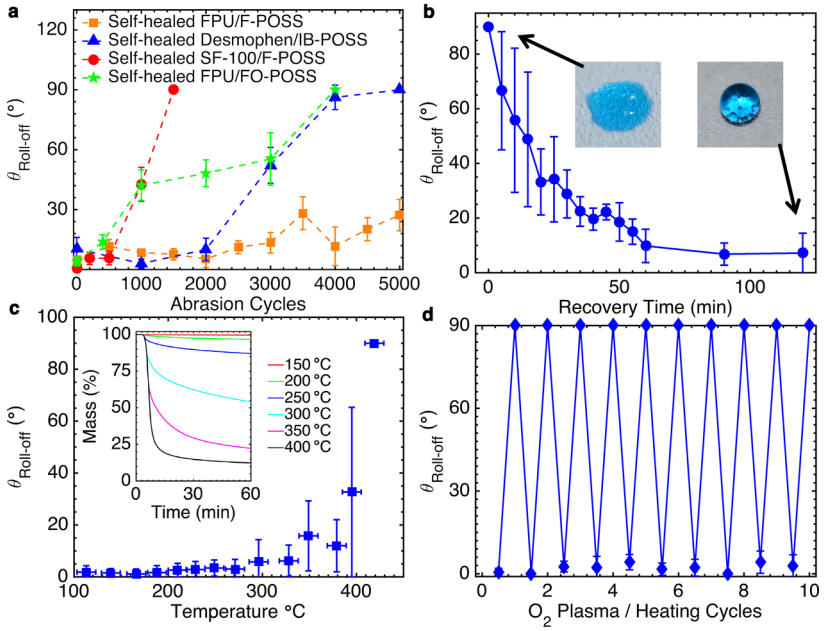

Figure 3. Self-healing SHSs. (a) Roll-off angle for four binder/filler blends after self-healing, as a function of the number of abrasion cycles. (b) Roll-off angle of the FPU+15 wt % F-POSS coating after O_2 plasma treatment, as a function of recovery time at 80 °C. As the fully fluorinated chains bloomed to the surface, the surface energy decreased, and water was more easily repelled. The insets show water droplets (dyed blue) after O_2 plasma treatment and after thermal recovery. (c) Roll-off angle of the FPU/F-POSS coating versus temperature held for 1 h. The inset shows TGA of the same coating at different temperature points. (d) Ten successive O_2 plasma/recovery cycles, which highlight that the self-healing nature of the FPU/F-POSS coating was quite robust.

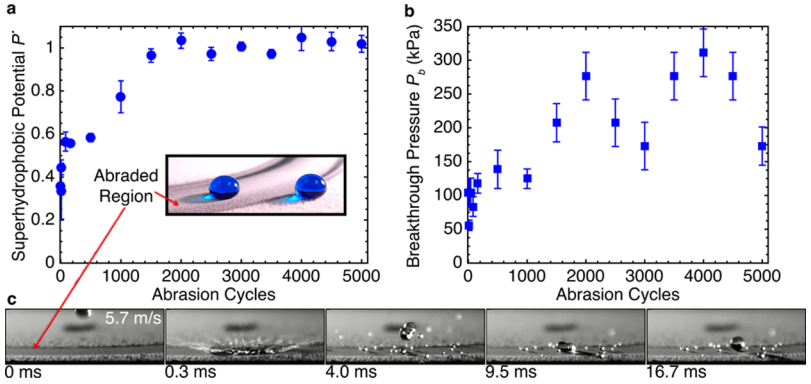

Figure 4. Capillary resistance. (a) P^* parameter as a function of the number of abrasion cycles for the FPU/F-POSS coating after self-healing. The inset shows water droplets (dyed blue) displaying high contact angle even after 5000 abrasion cycles. (b) Breakthrough pressure of the FPU/F-POSS coating as a function of abrasion after self-healing. (c) Water droplet, dropped from a height of ~1.7 m, impacts the abraded region (4000 abrasion cycles) of the FPU/F-POSS coating at a velocity of 5.7 m/s (see Movie 1). After breaking up, the satellite droplet bounces at least four times after impacting the surface. The surface is tilted at 1.5°.

coating was placed on a hot plate for a few minutes, the water repellency was easily restored ($\theta_{roll\text{-}off}$ < 5°, Figure 3a). With self-healing, the FPU/F-POSS coating maintained $\theta_{roll\text{-}off}$ < 15 even after 4000 abrasion cycles. Other blends created using different elastomers, such as SF-100/F-POSS, FPU/FO-POSS, or Desmophen 670BA/IB-POSS, also exhibited a self-healing nature. The self-healing and superhydrophobic nature of Desmophen 670BA/IB-POSS system is notable because neither of the components contains any fluorinated species.

The low surface energy of F-POSS causes it to migrate to the solid/air interface[59] and impart different binder/F-POSS blends with a robust, self-healing nature. For example, oxygen plasma, which has the capability of hydrolyzing F-POSS,[61] rendered the FPU/F-POSS coating hydrophilic within minutes (θ^* = 0°, although P^* remained unchanged). However, upon heating, the low surface energy was fully restored (Figure 3b). We found that the time required for full superhydrophobic recovery decreased with increasing temperature, consistent with a diffusion-controlled process. The coating maintained low $\theta_{roll\text{-}off}$ when held at temperatures up to about 400 °C, the point at which F-POSS begins to degrade (Figure 3c). However, even when >75% of the mass had degraded, the coating maintained $\theta_{roll\text{-}off}$ < 15°. We also repeatedly treated the coating with O_2 plasma and found that the water repellency was fully recovered by heating even after 10 successive treatments (Figure 3d).

Even after mechanical wear, a robust SHS should also exhibit a large capillary resistance or breakthrough pressure, P_b, defined as the pressure required to force a transition from the Cassie–Baxter to the Wenzel state.[10,11,52,62−64] Although the FPU/F-POSS coating maintained P^* < 1.0 over 5000 abrasion cycles

DOI: 10.1021/acsami.6b15491
ACS Appl. Mater. Interfaces 2017, 9, 11212−11223

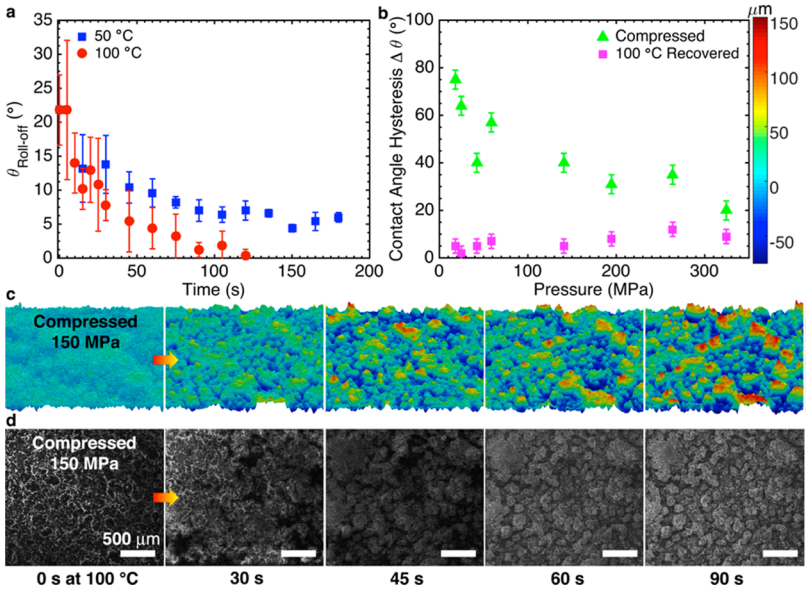

Figure 5. Texture recovery. (a) Self-healing properties of the FPU/F-POSS coating as a function of time and temperature, after 1000 Taber abrasion cycles. S_q increased from 2.6 to 3.3 μm during self-healing. (b) Contact angle hysteresis for the FPU/F-POSS coating before and after thermal recovery from compression, as a function of the compressive load. Note that the compressed coating's hysteresis decreased with an increase in applied load because the surface became smoother after compression. All compressed surfaces were fully wetted. (c) Height maps of the FPU/F-POSS coating after 150 MPa compression, as a function of recovery time at 100 °C. (d) Recovery of the texture was also imaged in situ using ESEM (Movie 2).

(Figure 4a), indicating an energetically favorable Cassie–Baxter state, a pressure-induced wetting transition is usually irreversible without some form of energy input.[10]

To evaluate the breakthrough pressure, we completely submerged our self-healed FPU/F-POSS coating in a pressurized water tank and observed when wetting occurred (Methods). The breakthrough pressure of this coating was initially P_b = 100 ± 20 kPa and never decreased below P_b = 50 kPa, even after 5000 abrasion cycles (Figure 4b). Remarkably, the pressure resistance increased to a maximum of P_b = 310 kPa after 4000 abrasion cycles due to the decrease in S_q with increasing abrasion. As such, even water droplets impinging the abraded surface at an impact velocity of ~6 m/s completely rebounded, which left the surface dry (Figure 4c and Movie 1). The maximum measured breakthrough pressure of 310 kPa corresponds to a droplet impact velocity of ~25 m/s ($P_{impact} = \rho V^2/2$) and a static water height of 31 m. Although often SHSs only maintain high contact angle after mechanical damage, the surfaces reported here preserve all their advantageous, water-repellant properties (high θ^*, $\theta_{roll\text{-}off}$ < 15°, high P_b) even after harsh mechanical abrasion.

The thermal recovery of low surface energy due to F-POSS migration will only result in a SHS if the texture is also maintained. Although abrasion damages the texture of the FPU/F-POSS coating, we found that the abraded texture was still sufficient for superhydrophobicity (Figure 4a). Further, we also observed that the texture could be partially restored during the thermal treatment. For example, after 1000 abrasion cycles, the FPU/F-POSS coating exhibited S_q = 2.6 μm. Thermal recovery at 100 °C for 120 s increased this value to S_q = 3.3 μm (measured at identical locations) (Figure 5a). Thus, abrasion also slightly compressed the coating. To further explore this, we subjected the coating to compressive stresses up to 350 MPa. Although flattening the texture elements significantly reduced the coating's porosity ($P^* \approx 2.0$, Figure 5b), such damage was reversible, and upon heating, the coating quickly recovered its original porous state ($P^* \approx 0.6$) (Figure 5b,c). Environmental scanning electron microscopy (ESEM) allowed us to observe this self-healing in situ (Figure 5d, Movie 2). As the compression set of elastomers is typically nonzero,[65,66] the use of elastomeric materials in the fabrication of SHSs may be advantageous in terms of their ability to recover from compressive stresses that flatten their porous texture, as shown here.

CONCLUSION

In summary, we have explored how miscibility between hydrophobic fillers and polymeric binders allows one to control the formation of surface texture during spray coating to fabricate superhydrophobic surfaces. The S^* parameter quantifies the miscibility between the two sprayable components, and the P^* parameter characterizes the stability of the nonwetted state. Superhydrophobic surfaces should be designed such that $S^* < 1.0$ to afford mechanical durability and $P^* < 1.0$ to provide a robust nonwetting state. Utilizing these two design criteria, we have fabricated superhydrophobic surfaces with unprecedented mechanical durability. Some of these surfaces also exhibited a self-healing nature, both chemically and physically, and were able to fully recover their superhydrophobicity after a wide variety of extreme chemical and physical exposures. These surfaces, and the design parameters used to develop them, may find immediate usage in a wide range of academic and industrial sectors across the globe.

METHODS

Materials. All solvents, prepolymers, and cross-linking agents were used as-received. Fluorinated solvents HCFC-225ca/cb (Asahiklin-225, Asahi Glass Co.) and HFC-43–10mee (Vertrel XF, DuPont) were purchased from Techspray and TMC Industries, Inc. respectively. Poly(methyl methacrylate) (PMMA), polystyrene (PS, 45 kDa or 1.2 kDa), and polyisobutylene (PIB) were purchased from

DOI: 10.1021/acsami.6b15491
ACS Appl. Mater. Interfaces 2017, 9, 11212–11223

Scientific Polymer. Luxecolor 4FVBA fluorinated polyol resin (55% solids in *n*-butyl acetate) was purchased from Helicity Technologies, Inc. Desmophen 670BA polyol was provided by Bayer MaterialScience, A.G. Isocyanate cross-linkers Desmodur N3200 and Wannate HMDI (4,4′-diisocyanato-methylenedicyclohexane) were provided by Bayer MaterialScience, A.G. and Wanhua Chemical Group Co., Ltd. respectively. Cross-linker ratios were 9.7 and 3.4 wt %, respectively, with FPU and 28.5 wt % N3200 with 670BA. Propylene glycol, a chain-extending agent that increases the modulus of the final cross-linked polyurethane network, was obtained from MP Biomedicals, LLC. A polyurethane elastomer (Vytaflex 40) was purchased from Smooth-On, Inc. and was prepared according to manufacturer directions. CNR (chlorinated polyisoprene) was provided by Covestro. Polydimethylsiloxane elastomer (Dow Corning Sylgard 184) was obtained from Krayden, Inc., and a 10:1 base/cross-linker ratio was used according to manufacturer directions. Acrylate-terminated perfluoropolyether resin (CN4001, purchased from Sartomer USA, LLC) was mixed with 5 wt % radical photoinitiator (Irgacure 2022, provided by BASF Corporation) to yield a UV-curable fluorinated polymer matrix. Cyanoacrylate adhesive (3 M Scotch-Weld SF100) was purchased from Pack-n-Tape, Inc. Two-part epoxy adhesive (Selleys Araldite 90 s) was used in an approximate 1:1 volume ratio of the components per manufacturer instructions.

Fluorodecyl and fluorooctyl polyhedral oligomeric silsesquioxanes (F-POSS, FO-POSS) were prepared by condensing perfluorinated triethoxysilanes as previously reported.[45] Octaisobutyl polyhedral oligomeric silsesquioxane (IB-POSS) was purchased from Hybrid Plastics, Inc. Eicosane was purchased from Acros Organics.

Coating Sample Fabrication. Spray coating solutions were prepared by solubilizing the filler, polymer, or prepolymer, and cross-linker or photoinitiator (if applicable) at an overall solution concentration of 100 mg/mL. The weight fraction of filler in the total solution was varied from 0 to 50%. The solvents used for F-POSS and FO-POSS blends were pure Vertrel XF (for FPU and PFPE), pure AK-225 (for SF100, 670BA, PMMA, chain-extended FPU, and PDMS), 50:50 chloroform/Vertrel XF (for Vytaflex 40, PS and Araldite epoxy), and 50:50 AK-225/hexane for PIB. Pure chloroform was used for IB-POSS blends with 670BA and FPU. Pure toluene was used for blends of eicosane and CNR.

No significant effect on spray coating morphology was observed between these solvents, as they have similar volatility and surface tension. The solutions were applied to 10 cm × 10 cm 6061 aluminum sheets with an ATD Tools 6903 high-volume−low-pressure spray gun. Twenty milliliters of coating solution was applied to each plate, which resulted in coatings that were approximately 100 μm thick. However, because the surfaces are both porous and extremely rough, the thickness could not be well-defined, and during abrasion tests, the mass % lost was tracked instead. Spray-coated samples were held at room temperature for at least 1 day and then cured as necessary prior to further testing (polyurethanes, 80 °C 2 days; PDMS, 150 °C 1 h; epoxy and cyanoacrylate, room temperature at least 2 h; PFPE acrylate resin, 15 min simultaneous exposure to 254 and 365 nm UV mercury lamp irradiation under N_2 atmosphere).

Hansen Solubility Parameter Studies. Hydrophobic filler miscibility in the polymer binders was analyzed with the aid of the HSPiP software package and associated database of Hansen solubility parameters. All solvents were used without further purification, including acetone, THF, chloroform, ethylene glycol, toluene, cyclohexane, hexane, dodecane, DMSO, ethanol, *n*-butyl acetate, MEK, and *o*-fluorotoluene (Fisher) as well as 1-hexanol, chlorobenzene, perfluorodecalin, hexafluorobenzene, *p*-chlorobenzotrifluoride, diisopropylamine, and pentafluorobutane (Sigma-Aldrich). Additionally, DI water, AK-225, and Vertrel XF were used.

Cross-linked polymers and elastomers were swollen in a selected number of solvents until a consistent mass was achieved. Samples were weighed, and then the solvent was extracted using a vacuum oven at 100 °C. The goodness of a solvent was determined by ranking the swelling ratio (divided by the mass of the solvent) from 1 to 6, with 1 being solvents that swell the polymer the most. These were then input into the HSPiP software to determine the center and radius of the given system or to determine other solvents necessary to better define the radius of the Hansen sphere.

The Hansen sphere for F-POSS was determined only using fluorinated solvents, as the fluorine−fluorine interaction is crucial in solubilizing the highly fluorinated compound.[45] As an example, hexafluorobenzene and dodecane have the exact same Hansen parameters and similar molecular volumes. However, F-POSS is completely insoluble in dodecane even at 1 mg/mL, whereas F-POSS is soluble up to 800 mg/mL in hexafluorobenzene. Thus, rather than confounding the results by including alkanes and other proximal molecules, only fluorinated solvents were used.

Along similar lines, the Hansen sphere for F-POSS was found for various solution concentrations. Although the Hansen radius is known to be weakly dependent on concentration,[43] we found a strong dependence when we evaluated fluorinated systems such as F-POSS (Figure S5b,c).

Wettability Measurements. Advancing and receding contact angle measurements were obtained via the sessile drop method using a Ramé-Hart 200 F1 contact angle goniometer. A water droplet suspended from a vertical dispensing needle was brought into contact with the substrate, and its volume increased and decreased to obtain the advancing and receding contact angles. A circular drop profile on the live video feed in the DROPImage Advanced software was used to obtain contact angle data. At least three points were measured for each surface at each abrasion condition. Droplet roll-off angles were obtained by placing at least five 25 μL water droplets distributed across the surface with a micropipette and using the manual tilting stage of the goniometer to gradually increase the angle. The tilt angle was recorded when each droplet rolled off, and the average across the droplets was calculated. Droplets that did not roll off were recorded as $\theta_{\text{roll-off}} = 90°$ for averaging purposes. The large error bars in some of the abraded samples in Figure 2 arose from averaging areas that wet with areas that remained superhydrophobic.

Abrasion Testing. Abrasion testing based on ASTM standard D4060 was performed with a Taber Model 5135 Rotary Abraser with CS-10 resilient abrasive wheels. Two-hundred-fifty gram weights were placed on the rear of the wheel arms such that the applied normal load was ∼60 g, and the sample was then rotated relative to the freely spinning abrasion wheels such that a shearing abrasion action occurred. Excess debris was removed continuously with a vacuum nozzle. The result was a circular region on the sample that was consistently mechanically damaged.

The manual sandpaper abrasion test performed previously[16] was automated using a Taber Model 5750 Linear Abraser. A 2.5 cm × 2.5 cm spray coated sample was mounted facing downward on the reciprocating head, and brought in contact with 240 grit sandpaper, with an applied load of ∼250 g. The sample was then moved under load on the static sandpaper, and the test was continued until water droplets were pinned. Water roll-off angles were measured periodically to confirm the retention of superhydrophobicity (Figure S2b).

Imaging and Metrology. Scanning electron micrographs were obtained with a Philips XL30 SEM after the samples were sputter coated with gold to reduce charging effects. Two-dimensional height-maps (2.4 mm × 2.4 mm) of the surfaces were obtained with an Olympus LEXT OLS4000 3D Laser Measuring Microscope with the 10× objective, and at least five were collected for each sample at each abrasion condition. These data were subsequently analyzed to yield statistical topographical parameters using MATLAB (see Supporting Information: Justification of Statistical Parameters).

Thermal Degradation Analysis. A sample of FPU+15 wt % F-POSS was placed on a hot plate at temperatures from 150−425 °C in increments of 25 °C, 1 h per temperature point. After each baking step, the advancing, receding, and roll-off angles were measured (Figure 3c). To correlate the onset of degradation of the Cassie−Baxter state with chemical degradation of the sample, thermogravimetric analysis was performed with a TA Instruments Discovery Series TGA using a 6 mg sample scraped from the same spray-coated surface. This sample was heated from 25−600 °C at 10 °C/min in a 10 mL/min N_2 gas purge flow while its mass was continually monitored (inset, Figure 3c).

DOI: 10.1021/acsami.6b15491
ACS Appl. Mater. Interfaces 2017, 9, 11212−11223

UV Exposure. A sample of FPU+15 wt % F-POSS was placed under 254 nm UVC mercury lamp (UVP, LLC) at a distance of 5 cm. The contact angles were measured after 5 h of continuous exposure.

O_2 Plasma Exposure. A sample of FPU+15 wt % F-POSS was exposed to O_2 plasma (Harrick Plasma PDC-001) using RF source power of 30 W and a pressure of ~200 mTorr for 20 min. Contact angles were measured to verify the complete wetting of the surface. To recover the water repellency, the coated surface was placed on a hot plate at a certain temperature (80 or 150 °C). For the time-dependent recovery, the substrate was removed from the hot plate after temporal increments, and the contact angles were measured. For the O_2 plasma cycling, the substrate was placed on a 150 °C hot plate for 20 min before contact angles were measured. The O_2 plasma exposure followed by the 150 °C recovery is denoted as one cycle in Figure 3d.

Corrosion Testing. Corrosion testing was done in accordance to ASTM B117. Briefly, steel tabs measuring 25 mm × 75 mm were spray-coated with the FPU+15 wt % F-POSS coating. The coated pieces were hung in a salt-spray fog chamber (Bemco Inc.) kept at 35 °C for 200 h. A 25 mm scratch was made along the length of the coating so that the steel underneath was exposed. After the accelerated corrosion, the contact angles were measured.

Compression Testing. Compression testing was done using a Carver 4350 compression molder with a 30 ton capacity. Samples of known dimensions were placed between aluminum plates, and a certain force was applied and held for 60 s. The contact angles were then measured immediately following compression. The coating was then self-healed on a 100 °C hot plate for 5 min, and contact angles were recorded again.

Breakthrough Pressure Testing/Droplet Impact. Pressure stability was measured both statically and dynamically. Static pressure testing was done using a pressure tank (TCP Global) with a 7 cm head of DI water. The pressure was regulated using compressed air. Samples were submerged, and the pressure was raised to the set level for 60 s at a ramp rate of no more than 5 psi per second. After the pressure was released, samples were removed to determine if they remained dry. Because of the inhomogeneity of the surfaces, breakthrough was considered to have occurred when the sample was fully wetted upon removal from the water tank.

Dynamic pressure testing was done using impacting water droplets and a high-speed camera (Fastec Imaging HiSpec 1) at 2000 fps. The breakthrough pressure was considered when the droplet became pinned on the surface upon impact. As the maximum droplet height for our experimental setup was 1.7 m, corresponding to an impact velocity of 5.7 m/s, many surfaces exhibited breakthrough pressures too high to measure using droplet impact.

■ ASSOCIATED CONTENT

Supporting Information

The Supporting Information is available free of charge on the ACS Publications website at DOI: 10.1021/acsami.6b15491.

Additional text, tables, and figures (PDF)
Movie 1 (AVI)
Movie 2 (AVI)
Movie 3 (AVI)
Movie 4 (AVI)

■ AUTHOR INFORMATION

Corresponding Author

*E-mail: atuteja@umich.edu.

ORCID

Anish Tuteja: 0000-0002-2383-4572

Author Contributions

K.G. and M.B. contributed equally. The manuscript was written through contributions of all authors. All authors have given approval to the final version of the manuscript.

Author Contributions

#Kevin Golovin and Mathew Boban contributed equally to this manuscript.

Notes

The authors declare no competing financial interest.

■ ACKNOWLEDGMENTS

We would like to thank Dr. Charles M. Hansen for the insightful comments. We thank Dr. Ki-Han Kim and the Office of Naval Research (ONR) for financial support under Grant No. N00014-12-1-0874. We also thank Dr. Charles Y. Lee and the Air Force Office of Scientific Research (AFOSR) for financial support under Grant Nos. FA9550-15-1-0329 and LRIR-12RZ03COR. We also thank the National Science Foundation and the Nanomanufacturing program for supporting this work through Grant No. 1351412. K.G. thanks the Department of Defense (DoD) for a National Defense Science & Engineering Graduate (NDSEG) Fellowship.

■ REFERENCES

(1) Bhushan, B.; Jung, Y. C. Natural and Biomimetic Artificial Surfaces for Superhydrophobicity, Self-Cleaning, Low Adhesion, and Drag Reduction. *Prog. Mater. Sci.* **2011**, *56* (1), 1−108.

(2) McHale, G.; Newton, M. I.; Shirtcliffe, N. J. Immersed Superhydrophobic Surfaces: Gas Exchange, Slip and Drag Reduction Properties. *Soft Matter* **2010**, *6* (4), 714.

(3) Liu, Y.; Liu, Z.; Liu, Y.; Hu, H.; Li, Y.; Yan, P.; Yu, B.; Zhou, F. One-Step Modification of Fabrics with Bioinspired Polydopamine@ Octadecylamine Nanocapsules for Robust and Healable Self-Cleaning Performance. *Small* **2015**, *11*, 426−431.

(4) Genzer, J.; Efimenko, K. Recent Developments in Superhydrophobic Surfaces and Their Relevance to Marine Fouling: A Review. *Biofouling* **2006**, *22* (5), 339−360.

(5) Tuteja, A.; Choi, W.; McKinley, G. H.; Cohen, R. E.; Rubner, M. F. Design Parameters for Superhydrophobicity and Superoleophobicity. *MRS Bull.* **2008**, *33* (8), 752.

(6) Im, M.; Im, H.; Lee, J.-H.; Yoon, J.-B.; Choi, Y.-K. A Robust Superhydrophobic and Superoleophobic Surface with Inverse-Trapezoidal Microstructures on a Large Transparent Flexible Substrate. *Soft Matter* **2010**, *6* (7), 1401.

(7) Maitra, T.; Antonini, C.; Auf der Mauer, M.; Stamatopoulos, C.; Tiwari, M. K.; Poulikakos, D. Hierarchically Nanotextured Surfaces Maintaining Superhydrophobicity Under Severely Adverse Conditions. *Nanoscale* **2014**, *6* (15), 8710−8719.

(8) Rykaczewski, K.; Osborn, W. A.; Chinn, J.; Walker, M. L.; Scott, J. H. J.; Jones, W.; Hao, C.; Yao, S.; Wang, Z. How Nanorough is Rough Enough to Make a Surface Superhydrophobic During Water Condensation? *Soft Matter* **2012**, *8* (33), 8786.

(9) Shen, L.; Qiu, W.; Liu, B.; Guo, Q. Stable Superhydrophobic Surface Based on Silicone Combustion Product. *RSC Adv.* **2014**, *4* (99), 56259−56262.

(10) Tuteja, A.; Choi, W.; Ma, M.; Mabry, J. M.; Mazzella, S. A.; Rutledge, G. C.; McKinley, G. H.; Cohen, R. E. Designing Superoleophobic Surfaces. *Science* **2007**, *318* (5856), 1618−1622.

(11) Tuteja, A.; Choi, W.; Mabry, J. M.; McKinley, G. H.; Cohen, R. E. Robust Omniphobic Surfaces. *Proc. Natl. Acad. Sci. U. S. A.* **2008**, *105* (47), 18200−18205.

(12) Verho, T.; Bower, C.; Andrew, P.; Franssila, S.; Ikkala, O.; Ras, R. H. Mechanically Durable Superhydrophobic Surfaces. *Adv. Mater.* **2011**, *23* (5), 673−678.

(13) Wang, F.; Yu, S.; Ou, J.; Xue, M.; Li, W. Mechanically Durable Superhydrophobic Surfaces Prepared by Abrading. *J. Appl. Phys.* **2013**, *114* (12), 124902.

(14) Wu, L.; Zhang, J.; Li, B.; Fan, L.; Li, L.; Wang, A. Facile Preparation of Super Durable Superhydrophobic Materials. *J. Colloid Interface Sci.* **2014**, *432*, 31−42.

DOI: 10.1021/acsami.6b15491
ACS Appl. Mater. Interfaces 2017, 9, 11212−11223

(15) Zhu, X.; Zhang, Z.; Men, X.; Yang, J.; Wang, K.; Xu, X.; Zhou, X.; Xue, Q. Robust Superhydrophobic Surfaces with Mechanical Durability and Easy Repairability. *J. Mater. Chem.* **2011**, *21* (39), 15793.
(16) Lu, Y.; Sathasivam, S.; Song, J.; Crick, C.; Carmalt, C.; Parkin, I. Robust Self-Cleaning Surfaces that Function when Exposed to Either Air or Oil. *Science* **2015**, *347* (6226), 1132−1135.
(17) Tian, X.; Verho, T.; Ras, R. H. Moving Superhydrophobic Surfaces Toward Real-World Applications. *Science* **2016**, *352* (6282), 142−143.
(18) Jiang, W.; Liu, H.; Wang, L.; Zhu, S.; Yin, L.; Shi, Y.; Chen, B.; Ding, Y.; An, N. An Effective Route for Transparent and Superhydrophobic Coating with High Mechanical Stability. *Thin Solid Films* **2014**, *562*, 383−388.
(19) Zhang, Y.; Ge, D.; Yang, S. Spray-Coating of Superhydrophobic Aluminum Alloys with Enhanced Mechanical Robustness. *J. Colloid Interface Sci.* **2014**, *423*, 101−107.
(20) Deng, X.; Mammen, L.; Butt, H. J.; Vollmer, D. Candle Soot as a Template for a Transparent Robust Superamphiphobic Coating. *Science* **2012**, *335* (6064), 67−70.
(21) Aytug, T.; Simpson, J. T.; Lupini, A. R.; Trejo, R. M.; Jellison, G. E.; Ivanov, I. N.; Pennycook, S. J.; Hillesheim, D. A.; Winter, K. O.; Christen, D. K.; et al. Optically Transparent, Mechanically Durable, Nanostructured Superhydrophobic Surfaces Enabled by Spinodally Phase-Separated Glass Thin Films. *Nanotechnology* **2013**, *24* (31), 315602.
(22) Li, Y.; Chen, S.; Wu, M.; Sun, J. All Spraying Processes for the Fabrication of Robust, Self-Healing, Superhydrophobic Coatings. *Adv. Mater.* **2014**, *26* (20), 3344−3348.
(23) Wang, H.; Liu, Z.; Zhang, X.; Lv, C.; Yuan, R.; Zhu, Y.; Mu, L.; Zhu, J. Durable Self-Healing Superhydrophobic Coating with Biomimic "Chloroplast" Analogous Structure. *Adv. Mater. Interfaces* **2016**, *3* (15), 1600040.
(24) Chen, L.; Sun, X.; Hang, J.; Jin, L.; Shang, D.; Shi, L. Large-Scale Fabrication of Robust Superhydrophobic Coatings with High Rigidity and Good Flexibility. *Adv. Mater. Interfaces* **2016**, *3* (6), 1500718.
(25) Infante, D.; Koch, K. W.; Mazumder, P.; Tian, L.; Carrilero, A.; Tulli, D.; Baker, D.; Pruneri, V. Durable, Superhydrophobic, Antireflection, and Low Haze Glass Surfaces Using Scalable Metal Dewetting Nanostructuring. *Nano Res.* **2013**, *6* (6), 429−440.
(26) Li, J.-H.; Weng, R.; Di, X.-Q.; Yao, Z.-W. Gradient and Weather Resistant Hybrid Super-Hydrophobic Coating Based on Fluorinated Epoxy Resin. *J. Appl. Polym. Sci.* **2014**, *131* (20), 40955−40962.
(27) Barthwal, S.; Kim, Y. S.; Lim, S. H. Mechanically Robust Superamphiphobic Aluminum Surface with Nanopore-Embedded Microtexture. *Langmuir* **2013**, *29* (38), 11966−11974.
(28) Lee, E. J.; Kim, J. J.; Cho, S. O. Fabrication of Porous Hierarchical Polymer/Ceramic Composites by Electron Irradiation of Organic/Inorganic Polymers: Route to a Highly Durable, Large-Area Superhydrophobic Coating. *Langmuir* **2010**, *26* (5), 3024−3030.
(29) Su, F.; Yao, K. Facile Fabrication of Superhydrophobic Surface with Excellent Mechanical Abrasion and Corrosion Resistance on Copper Substrate by a Novel Method. *ACS Appl. Mater. Interfaces* **2014**, *6* (11), 8762−8770.
(30) Yin, L.; Yang, J.; Tang, Y.; Chen, L.; Liu, C.; Tang, H.; Li, C. Mechanical Durability of Superhydrophobic and Oleophobic Copper Meshes. *Appl. Surf. Sci.* **2014**, *316*, 259−263.
(31) Dyett, B. P.; Wu, A. H.; Lamb, R. N. Mechanical Stability of Surface Architecture-Consequences for Superhydrophobicity. *ACS Appl. Mater. Interfaces* **2014**, *6* (21), 18380−18394.
(32) Esteves, A. C. C.; Luo, Y.; van de Put, M. W. P.; Carcouët, C. C. M.; de With, G. Self-Replenishing Dual Structured Superhydrophobic Coatings Prepared by Drop-Casting of an All-In-One Dispersion. *Adv. Funct. Mater.* **2014**, *24* (7), 986−992.
(33) Ma, J.; Zhang, X. Y.; Wang, D. P.; Zhao, D. Q.; Ding, D. W.; Liu, K.; Wang, W. H. Superhydrophobic Metallic Glass Surface with Superior Mechanical Stability and Corrosion Resistance. *Appl. Phys. Lett.* **2014**, *104* (17), 173701.
(34) Nine, M. J.; Cole, M. A.; Johnson, L.; Tran, D. N.; Losic, D. Robust Superhydrophobic Graphene-Based Composite Coatings with Self-Cleaning and Corrosion Barrier Properties. *ACS Appl. Mater. Interfaces* **2015**, *7* (51), 28482−28493.
(35) Chen, B.; Qiu, J.; Sakai, E.; Kanazawa, N.; Liang, R.; Feng, H. Robust and Superhydrophobic Surface Modification by a "Paint + Adhesive" Method: Applications in Self-Cleaning after Oil Contamination and Oil-Water Separation. *ACS Appl. Mater. Interfaces* **2016**, *8* (27), 17659−17667.
(36) Wong, W. S.; Stachurski, Z. H.; Nisbet, D. R.; Tricoli, A. Ultra-Durable and Transparent Self-Cleaning Surfaces by Large-Scale Self-Assembly of Hierarchical Interpenetrated Polymer Networks. *ACS Appl. Mater. Interfaces* **2016**, *8* (21), 13615−13623.
(37) Yuan, R.; Wu, S.; Yu, P.; Wang, B.; Mu, L.; Zhang, X.; Zhu, Y.; Wang, B.; Wang, H.; Zhu, J. Superamphiphobic and Electroactive Nanocomposite toward Self-Cleaning, Antiwear, and Anticorrosion Coatings. *ACS Appl. Mater. Interfaces* **2016**, *8* (19), 12481−12493.
(38) Gong, D.; Long, J.; Jiang, D.; Fan, P.; Zhang, H.; Li, L.; Zhong, M. Robust and Stable Transparent Superhydrophobic Polydimethylsiloxane Films by Duplicating via a Femtosecond Laser-Ablated Template. *ACS Appl. Mater. Interfaces* **2016**, *8* (27), 17511−17518.
(39) Steele, A.; Nayak, B. K.; Davis, A.; Gupta, M. C.; Loth, E. Linear Abrasion of a Titanium Superhydrophobic Surface Prepared by Ultrafast Laser Microtexturing. *J. Micromech. Microeng.* **2013**, *23* (11), 115012.
(40) Tian, X.; Shaw, S.; Lind, K. R.; Cademartiri, L. Thermal Processing of Silicones for Green, Scalable, and Healable Superhydrophobic Coatings. *Adv. Mater.* **2016**, *28* (19), 3677−3682.
(41) Lv, T.; Cheng, Z.; Zhang, E.; Kang, H.; Liu, Y.; Jiang, L. Self-Restoration of Superhydrophobicity on Shape Memory Polymer Arrays with Both Crushed Microstructure and Damaged Surface Chemistry. *Small* **2017**, *13*, 1503402.
(42) Wang, H.; Xue, Y.; Ding, J.; Feng, L.; Wang, X.; Lin, T. Durable, Self-Healing Superhydrophobic and Superoleophobic Surfaces From Fluorinated-Decyl Polyhedral Oligomeric Silsesquioxane and Hydrolyzed Fluorinated Alkyl Silane. *Angew. Chem., Int. Ed.* **2011**, *50* (48), 11433−11436.
(43) Wang, X.; Liu, X.; Zhou, F.; Liu, W. Self-healing Superamphiphobicity. *Chem. Commun. (Cambridge, U. K.)* **2011**, *47* (8), 2324−2326.
(44) Schulman, F.; Zisman, W. A. The Spreading of Liquids on Low-Energy Surfaces. V. Perfluorodecanoic Acid Monolayers. *J. Colloid Sci.* **1952**, *7* (5), 465−481.
(45) Mabry, J. M.; Vij, A.; Iacono, S. T.; Viers, B. D. Fluorinated Polyhedral Oligomeric Silsesquioxanes (F-POSS). *Angew. Chem., Int. Ed.* **2008**, *47* (22), 4137−4140.
(46) Shirtcliffe, N. J.; McHale, G.; Newton, M. I.; Perry, C. C. Intrinsically Superhydrophobic Organosilica Sol−Gel Foams. *Langmuir* **2003**, *19* (14), 5626−5631.
(47) Hansen, C. M. *Hansen Solubility Parameters: A User's Handbook*, 2nd ed.; CRC Press: Boca Raton, FL, 2007; p 519.
(48) Bottiglione, F.; Carbone, G. Role of Statistical Properties of Randomly Rough Surfaces in Controlling Superhydrophobicity. *Langmuir* **2013**, *29* (2), 599−609.
(49) Cassie, A. B. D.; Baxter, S. Wettability of Porous Surfaces. *Trans. Faraday Soc.* **1944**, *40*, 546−551.
(50) Wenzel, R. N. Resistance of Solid Surfaces to Wetting by Water. *Ind. Eng. Chem.* **1936**, *28* (8), 988.
(51) Davim, J. P. *Surface Integrity in Machining*; Springer: New York, 2009; Vol. *xii*, p. 215.
(52) Bico, J.; Thiele, U.; Quéré, D. Wetting of Textured Surfaces. *Colloids Surf., A* **2002**, *206* (1−3), 41−46.
(53) Tadmor, R. Line Energy and the Relation between Advancing, Receding, and Young Contact Angles. *Langmuir* **2004**, *20*, 7659−7664.
(54) de Gennes, P. G.; Brochard-Wyart, F.; Quéré, D. *Capillarity and Wetting Phenomena: Drops, Bubbles, Pearls, Waves*; Springer, 2004.
(55) Golovin, K.; Lee, D. H.; Mabry, J. M.; Tuteja, A. Transparent, Flexible, Superomniphobic Surfaces with Ultra-Low Contact Angle Hysteresis. *Angew. Chem., Int. Ed.* **2013**, *52* (49), 13007−13011.

DOI: 10.1021/acsami.6b15491
ACS Appl. Mater. Interfaces 2017, 9, 11212−11223

(56) Yang, J.; Zhang, Z.; Xu, X.; Men, X.; Zhu, X.; Zhou, X. Superoleophobic Textured Aluminum Surfaces. *New J. Chem.* **2011**, *35* (11), 2422.
(57) Guo, F.; Su, X.; Hou, G.; Li, P. Bioinspired Fabrication of Stable and Robust Superhydrophobic Steel Surface with Hierarchical Flowerlike Structure. *Colloids Surf., A* **2012**, *401*, 61−67.
(58) Campos, R.; Guenthner, A. J.; Meuler, A. J.; Tuteja, A.; Cohen, R. E.; McKinley, G. H.; Haddad, T. S.; Mabry, J. M. Superoleophobic Surfaces through Control of Sprayed-On Stochastic Topography. *Langmuir* **2012**, *28* (25), 9834−9841.
(59) Kota, A. K.; Kwon, G.; Choi, W.; Mabry, J. M.; Tuteja, A. Hygro-Responsive Membranes for Effective Oil-Water Separation. *Nat. Commun.* **2012**, *3*, 1025.
(60) Hertz, H. On the Contact of Elastic Solids. *J. Reine Angew. Math.* **1882**, *92*, 156−171.
(61) Kobaku, S. P.; Kota, A. K.; Lee, D. H.; Mabry, J. M.; Tuteja, A. Patterned Superomniphobic-Superomniphilic Surfaces: Templates for Site-Selective Self-Assembly. *Angew. Chem., Int. Ed.* **2012**, *51* (40), 10109−10113.
(62) Reyssat, M.; Pépin, A.; Marty, F.; Chen, Y.; Quéré, D. Bouncing Transitions on Microtextured Materials. *Europhys. Lett.* **2006**, *74* (2), 306−312.
(63) Di Mundo, R.; Bottiglione, F.; Carbone, G. Cassie State Robustness of Plasma Generated Randomly Nano-Rough Surfaces. *Appl. Surf. Sci.* **2014**, *316*, 324−332.
(64) Bottiglione, F.; Di Mundo, R.; Soria, L.; Carbone, G. Wenzel to Cassie Transition in Superhydrophobic Randomly Rough Surfaces. *Nanosci. Nanotechnol. Lett.* **2015**, *7* (1), 74−78.
(65) Drobny, J. G. Thermoplastic Polyurethane Elastomers. In *Handbook of Thermoplastic Elastomers*, 2nd ed.; William Andrew Publishing: Oxford, 2014; pp 233−253.
(66) Jaunich, M.; Stark, W.; Wolff, D. Comparison of Low Temperature Properties of Different Elastomer Materials Investigated by a New Method for Compression Set Measurement. *Polym. Test.* **2012**, *31* (8), 987−992.

DOI: 10.1021/acsami.6b15491
ACS Appl. Mater. Interfaces 2017, 9, 11212−11223